GEOPHYSICS, VOL. 72, NO. 2 (MARCH-APRIL 2007); P. S113–S122, 14 FIGS.
10.1190/1.2436845

Image-space surface-related multiple prediction

Brad Artman[1], Gabriel Alvarez[1], and Ken Matson[2]

ABSTRACT

A very important aspect of removing multiples from seismic data is accurate prediction of their kinematics. We cast the multiple prediction problem as an operation in the image space parallel to the conventional surface-related multiple-prediction methodology. Though developed in the image domain, the technique shares the data-driven strengths of data-domain surface-related multiple elimination (SRME) by being independent of the earth (velocity) model. Also, the data are used to predict the multiples exactly so that a Radon transform need not be designed to separate the two types of events. The cost of the prediction is approximately the same as that of data-space methods, though it can be computed during the course of migration. The additional cost is not significant compared to that incurred by shot-profile migration, though split-spread gathers must be used. Image-space multiple predictions are generated by autoconvolving the traces in each shot-gather at every depth level during the course of a shot-profile migration. The prediction in the image domain is equivalent to that produced by migrating the data-space convolutional prediction. Adaptive subtraction of the prediction from the image is required. Subtraction in the image domain, however, provides the advantages of focused energy in a smaller domain since extrapolation removes some of the imperfections of the input data.

INTRODUCTION

Removing multiples from seismic data is often an imperative to producing interpretable images of the subsurface. Multiple attenuation has a rich history in the geophysical literature ranging from methods that predict the multiples via convolution of the data (Anstey and Newman, 1966) to methods that use a differential characteristic between primaries and multiples as a discriminator for separating the two types of events (Hampson, 1986; Weglein, 1999).

Kinematic prediction of multiple reflections by convolution leads to amplitude and bandwidth inconsistencies. Therefore, direct subtraction of such predictions is not possible. Tsai (1985) suggests modeling the waveform of the multiples to subtract events at times calculated by convolution from the data. The surface-related multiple elimination (SRME) method (Verschuur et al., 1992; Berkhout and Verschuur, 1997) convolves traces within shot-gathers to predict multiples (surface-related multiple prediction, SRMP) followed by an iterative subtraction scheme to eliminate them from the data. Alternatively, after predicting multiples, via convolution or filter-based methods, Guitton (2005) uses a pattern-based subtraction technique that resembles the match filter application described in Biersteker (2001).

While the above references all operate in the data domain, authors have also suggested removing multiples in the image space, after migration (Sava and Guitton, 2003, 2005; Alvarez et al., 2004). These authors capitalize on kinematic differentiation of the primaries and multiples and separate the two via a Radon transform tailored to residual moveout or the analytic expression of over-migrated multiples, respectively. There are several motivators for attacking multiples in the image space. First, the image space is usually much smaller than the data space. Second, given a reasonably accurate velocity model, the kinematics of the image domain are simplified. Appropriately migrated primary events have little to no residual moveout, and multiples, migrated with velocities that are too fast, have predictable moveout in both angle- and offset-domain common-image gathers. Alternatively, one could migrate the data and a data-domain multiple prediction separately and subtract the two image volumes. This may be a prohibitively expensive strategy. However, null-traces in the data are filled during extrapolation steps as energy propagates laterally during downward continuation. This may help multiple predictions in the image space to be more continuous and accurate in 3D.

We extend the SRMP approach to the image domain through the commutability of wavefield extrapolation and convolution to produce a multiple prediction in the image domain without needing to migrate two data volumes. Our approach is directly analogous to SRMP, though the prediction is calculated during the course of a

Manuscript received by the Editor July 13, 2006; revised manuscript received October 9, 2006; published online February 26, 2007.
[1]Stanford University, Stanford Exploration Project, Department of Geophysics, Stanford, California. E-mail: brad@sep.stanford.edu.
[2]BP, Houston, Texas. E-mail: matsonkh@bp.com.

shot-profile migration. The added cost of image-space surface-related multiple prediction (IS-SRMP) is only a second imaging-condition. Because extrapolation dominates the cost of shot-profile migration, IS-SRMP does not significantly increase its cost.

Muijs (2005) develops an analogous strategy to IS-SRMP. That work requires substantial preprocessing, as its input is a previous migration result. Furthermore, the imaging procedure uses a multidimensional Fourier domain (transformed over source position) deconvolutional imaging condition that is iteratively performed over frequency and position that would seem very computationally burdensome. Generating a multiple model in the image domain during survey-sinking migrations was also discussed in Malcolm et al. (2007). Because the upcoming and downgoing energy are not explicitly separate, as in shot-profile algorithms, the authors require extra work that is not necessary for this method. That extra work effectively doubles the cost and memory requirements of the (DSR) migration. In contrast to our method, it implicitly acts as a layer-stripping methodology that is also capable of predicting intrabed multiples.

The multiple prediction produced in the image space with this technique is mathematically equivalent to migrating the multiple prediction produced by SRMP convolutions. The predicted multiples are then removed from the data via adaptive subtraction or pattern-matching techniques. The need for adaptive subtraction is twofold. First, convolution squares the wavelet in the data which reduces the effective bandwidth, squares the amplitude, and alters the polarity of the output. Therefore, even if a true-amplitude migration algorithm is available, the multiple prediction will not share the amplitude characteristics of the multiples in the migrated image. Second, adaptive subtraction can account for imperfections including kinematic errors or the presence of higher-order multiples in the prediction.

As wave-equation migration becomes more of a commodity, iterative migration as part of estimating the earth's velocity has become more common. The presence of multiples in the data makes velocity analysis more difficult since events with conflicting velocity properties are present at the same time or depth. For this reason, there will always be a need to remove multiples in the data domain. However, if a shot-profile migration strategy is planned, it will be shown that simultaneously producing a multiple prediction adds no significant cost, and does not require the presence of multiples in the data being migrated. Therefore, the prediction can be generated even after perfect elimination as a comparative volume for interpreters to use as an example of events that are not geologic.

In this paper, we develop the image-space surface-related multiple prediction (IS-SRMP) technique by combining the SRMP approach with a wave-equation shot-profile depth migration algorithm. Guitton (2005) shows that pattern-based and adaptive subtraction of multiple models work better when higher dimensionalities can be exploited by the subtraction algorithm. The various imaging conditions we present can all produce the image as a function of subsurface offset (and from there reflection angle) to facilitate better subtraction. A simple flat-layer synthetic and the Sigsbee2B synthetic data set are used to show the efficacy of the prediction and its subtraction from the migrated image. Multiple prediction and subtraction is also presented with a Gulf of Mexico data set acquired by Western-Geco in the Mississippi Canyon lease area.

THEORY

The image space is the output of migration, which we produce with a shot-profile depth migration algorithm. Shot-profile wave-equation depth migration (Claerbout, 1971) is the cascade of two component operations: extrapolation and imaging. Extrapolation is carried out with an anticausal wave-equation operator applied to the upgoing wavefield, U, and a causal operator applied to the down-going wavefield, D. U is a shot record with traces placed along a wavefield axis $\mathbf{x}$. D is a zero-valued wavefield, also defined along the axis $\mathbf{x}$, where a source function is placed at the location of the shot being migrated, $\mathbf{x}_s$. The wavefields are recursively extrapolated to all depths z using one-way mixed-domain solutions to the wave-equation

$$U_{z+1}(\mathbf{x};\mathbf{x}_s,t) = E^{+}(\mathbf{x},t)U_z(\mathbf{x},\mathbf{x}_s,t) \tag{1}$$

and

$$D_{z+1}(\mathbf{x};\mathbf{x}_s,t) = E^{-}(\mathbf{x},t)D_z(\mathbf{x};\mathbf{x}_s,t). \tag{2}$$

In this work, the form of the extrapolator E used to propagate the wavefields is the split-step Fourier plus interpolation algorithm (SSF-PI) (Kessinger, 1992) with multiple reference velocities, though the degree of complexity of the operator does not change the discussion herein. The importance of these equations is that the one-way operators and the wavefields they are applied to are independant components of the seismic experiment. Therefore, wavefields can be redatumed with appropriate extrapolators and combined, via correlation, at any subsurface level with an imaging condition.

The correlation-based multioffset imaging condition for shot-profile migration is (Rickett and Sava, 2002)

$$i_z(\mathbf{x},\mathbf{h}) = \sum_{\mathbf{x}_s}\sum_{\omega} U_z(\mathbf{x}+\mathbf{h};\mathbf{x}_s,\omega)D_z^{*}(\mathbf{x}-\mathbf{h};\mathbf{x}_s,\omega), \tag{3}$$

where the $*$ represents conjugation, and $\mathbf{h}$ is subsurface offset. Extraction of the zero lag of the correlations, by summation over ω, combines the energy in the two wavefields that is collocated at each depth level. Overlapping acquisition patches from the individual shots are stacked by the sum over $\mathbf{x}_s$.

Acknowledging the approximation of convolving raw data traces in lieu of only primaries, the prediction of multiples in the data space (SRMP) can be written in the Fourier domain (Berkhout and Verschuur, 1997 equation 13)

$$M(\mathbf{x}_g;\mathbf{x}_s,\omega) = \sum_{\mathbf{x}_a} R(\mathbf{x}_g;\mathbf{x}_a,\omega)R(\mathbf{x}_a;\mathbf{x}_s,\omega) \tag{4}$$

where R is the data-space volume of shot-gathers defined at geophone and source locations on the acquisition surface. Equation 4 is a trace-by-trace operation to produce the multiple prediction with any geophone-source combination $(\mathbf{x}_g,\mathbf{x}_s)$, by convolving each trace of every shot gather with all the others followed by summing over the convolution index $\mathbf{x}_a$. Note however, the similarity of the SRMP equation to the imaging condition of shot-profile migration, equation 3.

Wave-equation extrapolation is performed on wavefields where data and source-functions are used as initial conditions to propagate energy into the subsurface. To begin, traces at locations $\mathbf{x}_g$ are inserted into a zero-valued wavefield defined along the axis $\mathbf{x}$. Although data-space SRMP is a trace-by-trace operation, equation 4 can be redefined in terms of the wavefield $U(\mathbf{x},\mathbf{x}_s)$. With null-traces at loca-

tions $\mathbf{x}$ where no data were collected, a multiple prediction can also be written

$$M_{z=0}(\mathbf{x};\mathbf{x}_s,\omega) = \sum_{\mathbf{x}_a} U_{z=0}(\mathbf{x};\mathbf{x}_a,\omega)U_{z=0}(\mathbf{x}_a;\mathbf{x}_s,\omega), \quad (5)$$

where the resultant volume has been regularized along $\mathbf{x}$ by adding zero-traces, and we have added the specification that the operation is being performed at the recording surface $z = 0$.

Using the principle of reciprocity between the receiver and source locations (first and second arguments of the wavefields, respectively), the multiple prediction becomes

$$M_{z=0}(\mathbf{x};\mathbf{x}_s,\omega) = \sum_{\mathbf{x}_a} U_{z=0}(\mathbf{x};\mathbf{x}_a,\omega)U_{z=0}(\mathbf{x}_s;\mathbf{x}_a,\omega). \quad (6)$$

Here, the subscript s on the RHS represents any different receiver location (since it is the first argument of the wavefield), and the dummy index $\mathbf{x}_a$ is recognized as a summation over source location. Therefore, using arbitrary index subscripts c,d and restoring the significance of source location to subscript s,

$$M_{z=0}(\mathbf{x}_c;\mathbf{x}_d,\omega) = \sum_{\mathbf{x}_s} U_{z=0}(\mathbf{x}_c;\mathbf{x}_s,\omega)U_{z=0}(\mathbf{x}_d;\mathbf{x}_s,\omega). \quad (7)$$

Finally, we define the dummy indices c,d in terms of physically significant variables location and half-offset, $\mathbf{x}_c = \mathbf{x} + \mathbf{h}$ and $\mathbf{x}_d = \mathbf{x} - \mathbf{h}$, such that

$$M_{z=0}(\mathbf{x},\mathbf{h},\omega) = \sum_{\mathbf{x}_s} U_{z=0}(\mathbf{x}+\mathbf{h};\mathbf{x}_s,\omega)U_{z=0}(\mathbf{x}-\mathbf{h};\mathbf{x}_s,\omega). \quad (8)$$

Thus, reconfigured equation 8 is now of parallel construction to the shot-profile imaging condition, equation 3, lacking only the summation over frequency.

Extrapolation by $E(\mathbf{x},\mathbf{t})$, in equation 1, simply redatums the shot-gather U. Image-space SRMP (IS-SRMP) is the application of a second imaging condition evaluated at each subsurface depth level during the migration that images only multiples. It is the chain of multiple prediction (convolution) and zero-time extraction (summation over frequency). The image-space multiple prediction, as a function of subsurface offset, is therefore

$$m_z(\mathbf{x},\mathbf{h}) = \sum_{\mathbf{x}_s}\sum_{\omega} U_z(\mathbf{x}+\mathbf{h};\mathbf{x}_s,\omega)U_z(\mathbf{x}-\mathbf{h};\mathbf{x}_s,\omega). \quad (9)$$

There are two important ramifications associated with the equation for predicting multiples with the imaging condition above. The first is that this operation is intrinsically a shot-domain manipulation of the data. After sorting to midpoint-offset coordinates, the source and receiver coordinates are mixed in such a way as to make IS-SRMP more difficult for survey-sinking style migration algorithms (Malcolm et al., 2007). Second, because reciprocity was invoked to derive equation 9, off-end (marine) acquisition geometries will need to have split-spread gathers generated via reciprocity. The split-spread gathers will include the raypaths from multiples that emerge in front of the receiver spread (boat) which need to be included in the shot-gathers to predict all possible multiple events.

Further understanding of the IS-SRMP imaging condition for those familiar with shot-profile migration algorithms can be elicited by defining the downgoing wavefield in equation 2 as $D \equiv U$. Therefore, equations 1-3 become

$$U_{z+1}(\mathbf{x};\mathbf{x}_s,t) = E^{-}(\mathbf{x},t)U_z(\mathbf{x};\mathbf{x}_s,t) \quad (10)$$

and

$$\hat{U}_{z+1}(\mathbf{x};\mathbf{x}_s,t) = E^{+}(\mathbf{x},t)\hat{U}_z(\mathbf{x};\mathbf{x}_s,t), \quad (11)$$

with the imaging condition

$$i_z(\mathbf{x},\mathbf{h}) = \sum_{\mathbf{x}_s}\sum_{\omega} U_z(\mathbf{x}+\mathbf{h};\mathbf{x}_s,\omega)\hat{U}_z^{*}(\mathbf{x}-\mathbf{h};\mathbf{x}_s,\omega), \quad (12)$$

where $\hat{}$ denotes that after extrapolation in different directions, the wavefields are no longer identical. Because the conjugation of D in the imaging condition of equation 3 can be commuted with the causality of the extrapolation operator, it is not necessary to extrapolate U in two different directions. Instead, the second extrapolation above can be ignored and the imaging condition becomes convolutional rather than correlational. In this case, equation 12 is exactly the multiple prediction, equation 9.

Cast in this manner, the migration shows similarity with reverse-time migration (Baysal et al., 1983) and using multiples to migrate primaries (Shan and Guitton, 2004). The difference is that the data used as source function is not first time-reversed. IS-SRMP uses the data as both areal source functions and data to image multiples. Conversely, time-reversing the data will use the primaries as areal source functions (delayed from time zero) to image the subsurface with the multiple reflections. Using both an impulsive source function at $\mathbf{x}_s$ and time-reversed primaries as a source function would image earth structure with the primaries and the multiples, but still include the multiples in the image.

Analytic example

In 1D, let a trace be represented in the Fourier domain by the expression

$$\begin{aligned} R(\omega) &= \mathrm{e}^{-i\phi_\infty} + \mathrm{e}^{-i\phi_e} - \mathrm{e}^{-i2\phi_\infty} - 2\mathrm{e}^{-i(\phi_\infty+\phi_r)} - \mathrm{e}^{-i2\phi_s} \\ &= P + M_1. \end{aligned} \quad (13)$$

The trace has primary reflections, P, at phase delays, ϕ, representing a water-bottom and a subsurface event. Also included are first-order multiples, M_1, which are the water-bottom multiple at $2\phi_w$, two pegleg multiples at $\phi_w + \phi_e$, and the event multiple at $2\phi_e$. SRMP dictates the autoconvolution of P to derive M_1, which is clearly true. Including the events M_1 in the autoconvolution will predict the higher-order multiples as well.

Extrapolating trace R to a deeper depth applies a common phase shift, say $\mathbf{e}^{-i\phi_z}$, to all terms in equation 13. The trace then becomes

$$\begin{aligned} R_z(\omega) &= e^{-i\phi_z}(\mathrm{e}^{-i\phi_\omega} + e^{-i\phi_s} + \mathrm{e}^{-i2\phi_w} + 2\mathrm{e}^{-i(\phi_w+\phi_e)} + \mathrm{e}^{-i2\phi_e}) \\ &= e^{-i\phi_z}P + e^{-i\phi_z}M_1. \end{aligned} \quad (14)$$

This equation shows that the extrapolation of data without multiple subtraction produces the super-position of the redatumed primaries and the redatumed multiples. The extraction of the zero-time lag in the imaging condition of migration states that energy in the wavefield should be mapped into the image domain only when the extrapolation phasor ϕ_z, is equal to the time delay of the event in the data. Thus, the water-bottom primary is imaged when $\phi_z = \phi_w$, the water-bottom multiple is imaged when $\phi_z = 2\phi_w$, etc. Whether the data R is first separated into its constituent parts, P and M_i, or not, it can be

seen where in the image domain the various events in the above example will be placed. However, by first squaring the trace, implementing data-space SRMP, the water-bottom primary is mapped into the image domain when $\phi_z = 2\phi_w$. This is the same phasor that maps the recorded water-bottom multiple into the image domain when migrating data contaminated with multiples.

Figure 1 is a cartoon depicting the generation of a 1D image-space surface-related multiple prediction without first convolving the gathers. The scenario drawn is for the simple case of a water-bottom reflector and its multiple. The trace U denotes a zero-offset recording from a shot gather, and D is the modeled source function used for shot-profile migration. The trace I represents the result of the conventional imaging condition, while M is the multiple prediction in the image space generated by autoconvolution. The superscript * denotes conjugation. Both imaging conditions extract energy only at $t = 0$.

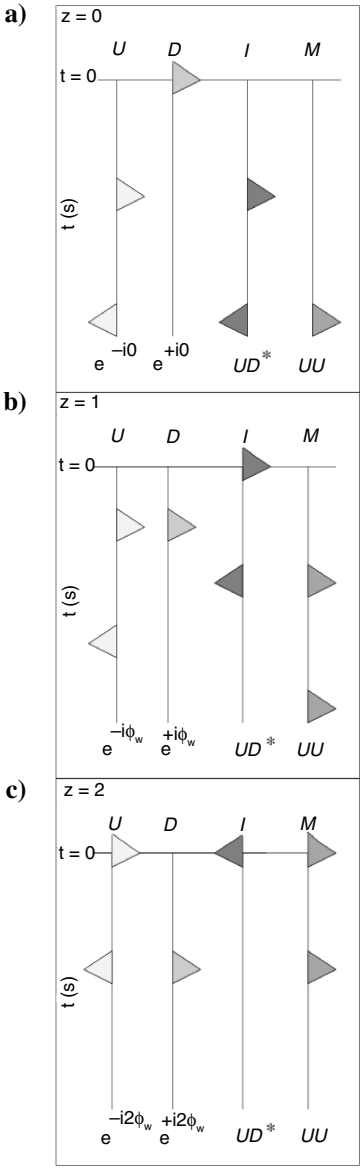

Figure 1. One-dimensional example of IS-SRMP during shot-profile migration at three extrapolation levels, (a) $z = 0$, (b) $z = 1$, (c) $z = 2$. Trace U represents data with a primary and multiple event. Trace D is the modeled impulsive source wavefield. Trace I is the conventional image (UD^*). Trace M is the multiple prediction (UU). Final image volumes for each depth level are produced by extracting the values of I and M at $t = 0$.

Figure 1a, $z = 0$, shows the initial conditions of U and D and the fact that both $I|_{t^* = 0}$ and $M|_{t = 0}$ are devoid of events. Since correlation subtracts the time to energy in the source trace D, currently zero, from the receiver trace, U, the image trace I is the same as U. The time for events on trace UU are doubled from the initial condition, which results in the multiple on trace U mapping below the time interval shown in the cartoon.

Figure 1b depicts the situation when the wavefields have been extrapolated to the depth of the water column. Now energy in D and U is collocated and the primary is imaged during correlation, UD^*. The multiple prediction is still zero valued. Figure 1c depicts the wavefields and imaging results after the wavefields have been propagated to twice the depth of the water column. Now the source energy is collocated with the multiple, and the correlation results in a negative polarity event. Simultaneously, the primary is now at $t = 0$ which maps energy into the IS-SRMP volume, M. However, even though the kinematics of the multiple in UU are correct, the event has the wrong polarity. Also notice that the multiple is now at the original time of the primary, which sets up prediction of second-order multiples from the convolution of the first-order multiples. Importantly, even if the velocity used to calculate the extrapolation phasors is incorrect, both I and M will share the same error. Also, U consisting of only primaries will correctly predict the location of first-order multiples even if no multiples exist in the data.

EXAMPLES

Simple synthetic

Figure 2a is a synthetic shot gather with two reflections and three multiples. The velocity to the first flat layer at depth $z = 400$ m is 1500 m/s. The velocity is 2500 m/s to the second flat layer at depth $z = 1200$ m. The traveltimes were computed analytically and convolved with a wavelet. The white events are primaries, and the multiples have opposite polarity. The three multiple events are the simple multiples to both events, and the asymmetric peg-leg. The intrabed multiples between the two layers were not included since they are not predicted by SRMP. Receiver and source spacing was 20 m. Fig-

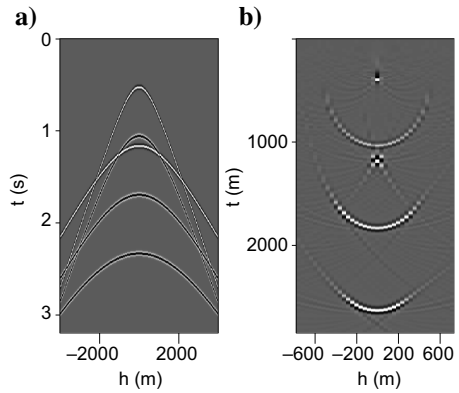

Figure 2. (a) Synthetic data with two primaries and three multiples. White events are primaries. Two simple and a peg-leg multiple were modeled. (b) Subsurface-offset common-image gather produced by shot-profile migration.

ure 2b is a subsurface-offset common-image gather produced by shot-profile migration of 350 shot-gathers identical to the data shown. Because the layers are flat, every location **x**, away from the edges, is the same. Only 1/6 of the subsurface offsets are required to capture the moveout of events after migration.

Figure 3a and b shows offset-domain common-image gathers produced by migrating only the primaries in the data above. Figure 3a shows energy tightly focused at zero offset for the two reflectors. Figure 3b is the multiple prediction. Three clear events are imaged with concave-up moveout. The middle event is the peg-leg multiple and the others are the simple multiples to the two reflectors. At zero offset, the events are analytically calculated to arrive at depths z = 1066, 1866, and 2666 m, respectively.

Figure 4a and b shows offset-domain common-image gathers produced by migrating all the events in Figure 2. Autoconvolution of primaries predicts first-order multiples. Convolution of primaries with multiples produces second-order, and higher, multiples. Figure 4a has the two focused primary events and the three multiples predicted by IS-SRMP in Figure 3. These multiples are again predicted in the IS-SRMP gather in Figure 4b. However, higher-order multiples are now predicted as well. The broad event at z = 1733 m is the multiple that makes three trips through the water column. The faint event at z = 2400 m is the double water-column multiple. The last new event is at z = 2533 m. This multiple has two trips in the water column and one trip from the surface to the second reflector. The predicted multiples (Figure 4b) all have very different amplitude than the multiples in Figure 4a. This is one of the main reasons direct subtraction of the prediction from the image is not possible.

Sigsbee2B synthetic

The Sigsbee2B data set was designed to model strong surface-related multiples from an offshore acquisition. Two data sets were generated with a 2D finite difference algorithm: one with the perfectly reflecting free surface, and one without.[2] Therefore, the direct subtraction of the two data volumes yields a nearly perfect multiple model without the need for SRMP. There are slight differences in the source and receiver ghost effects between the two data sets, so their subtraction retains faint residuals of primary energy. Though the data were modeled with an off-end acquisition strategy, split-spread gathers were computed via reciprocity for all of the examples below. All of the images herein were produced with four reference velocities in an SSF-PI shot-profile migration code.

Figure 5 shows zero subsurface-offset images of the Sigsbee2B data set. Figure 5a, generated with the conventional imaging condition, contains primaries and multiples. Figure 5b has multiples and some migration artifacts. The worst artifacts in the prediction are above the first multiple, especially near steep salt flanks. This noise can be easily muted before subtraction. The IS-SRMP image was produced using the data with primaries only. The data were modeled such that the details of the bottom left corner have simple kinematic differences between primaries and multiples: events dipping up-right are multiples, and those dipping down-right are primaries.

Figure 6 shows the bottom third of the image produced with the Sigsbee2B data sets. Figure 6a was produced with the data modeled without the reflecting free surface and contains only primaries. Figure 6b was produced with data modeled with the free surface and contains multiples. Figure 6c is the image produced by migrating the difference between the two modeled data volumes (only multiples). The complex multiples in this deep section quickly overwhelm the primary events and could easily be mistaken for primaries in some instances. Notice the faint primaries in the top left corner and the basement reflector due to the imperfect subtraction. Figure 6d is a zoomed-in version of the image-space multiple prediction in Figure 5. No residual primaries are present, but some edge effects are visible at z = 6 km on the left side. Figure 6c is effectively identical with Figure 6d which demonstrates the commutability of SRMP convolutions and shot-profile migration.

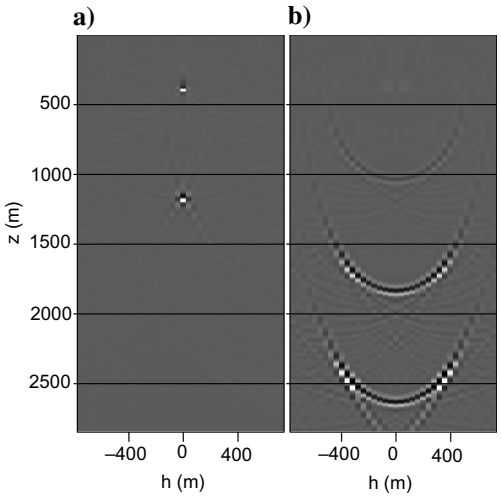

Figure 3. Offset-domain common-image gathers from migrating only the primaries in Figure 2. (a) Conventional imaging condition. (b) IS-SRMP.

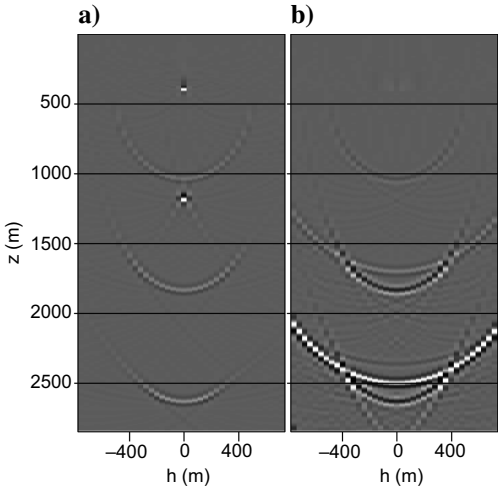

Figure 4. Offset-domain common-image gathers from migrating all events in Figure 2. (a) Conventional imaging condition. (b) IS-SRMP with higher-order multiples.

[2]http://www.delphi.tudelft.nl/SMAART/B2Breadme.htm.

Gulf of Mexico data

Figure 7a is a shot gather from a data set acquired in 1997 by Western-Geco in the Mississippi Canyon lease area of the Gulf of Mexico. Split-spread coverage was generated via reciprocity. The data set contains 1096 shots and recorded to 10 s. The source and receiver sampling was 27 m. Figure 7b is a migrated angle gather from the same location. The raw data contains 367 traces, although the angle gather contains only 60 traces. Primaries arc flat, and multiples arc characteristically concave-down. Before migration, the data were regularized, and band-passed from 3–65 Hz. The data were migrated with the same SSF-PI shot-profile migration algorithm with four reference velocities. To produce only the zero-subsurface offset of the prestack migration, the cost of the imaging condition, including the multiple prediction, was 1.4% of the cost of extrapolation. Calculating 60 subsurface offsets approximately equalizes the costs of extrapolation (with four reference velocities) and imaging (including multiple prediction and conventional image generation). This number of offsets is about 1/6 of the traces in the split-spread gather, and more than sufficient to capture the unfocused multiple energy at all depths in the subsurface-offset gathers.

Figure 8 shows (a) the resulting migration and (b) image-space multiple prediction. The multiples have the opposite polarity as expected. The quantity of multiple events in the prediction is overwhelming. Several events in the deep section of the image that have correspondence in the multiple prediction, look very much like primaries. The short, faint event that runs off the bottom of the image at $x = 2$ km could very easily be misinterpreted as a primary. Below the salt bottom and above the first water-bottom multiple, several intrabed multiples can be identified in the image that are not predicted in this context.

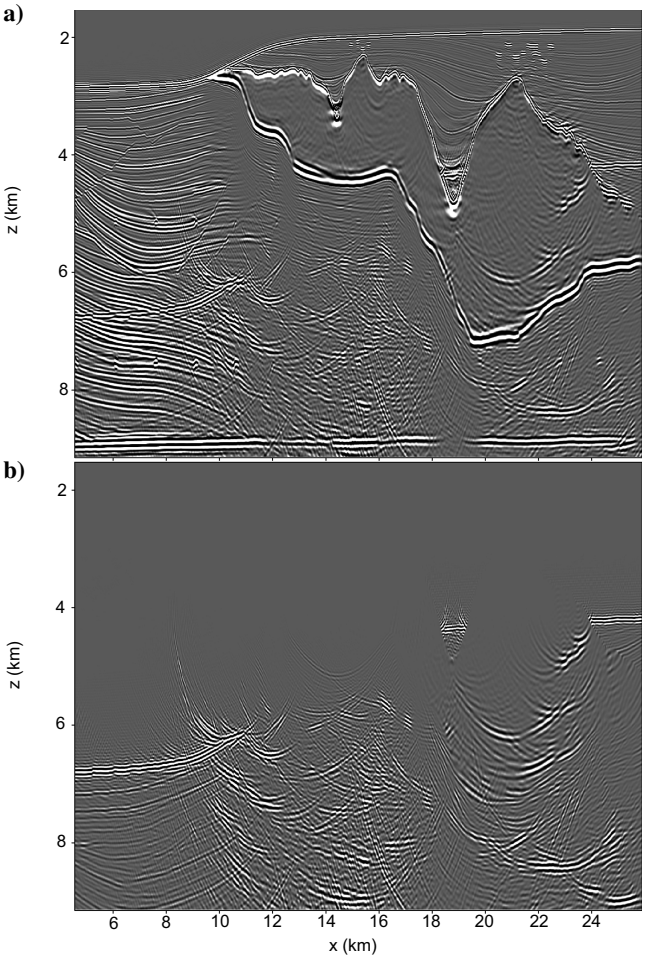

Figure 5. (a) Migration of the Sigsbee2B data containing multiples, and (b) the IS-SRMP result using data containing only primaries.

ADAPTIVE SUBTRACTION

After predicting the kinematics of the multiples, they must be adaptively subtracted from the image due to the amplitude and bandwidth problems associated with convolving the traces. Another potential problem with generating a multiple prediction by convolving data instead of only the primaries is the prediction of higher-order multiples with increasing amplitude increases. The adaptive subtraction must be able to adjust the amplitude and phase of the prediction to the image, and ignore events in the multiple prediction that are completely absent from the data. Also, the multiple prediction has more artifacts than the image. This is especially true at shallow depths before the first multiple. These artifacts must not be allowed to damage the primary energy in the image.

We present subtraction results from the previous predictions using adaptive subtraction. Adaptive subtraction proceeds by inverting for match filters connecting two similar objects, convolving the filters with its object, and subtracting this result from the second object. This can be a complicated and subtle art that we make no claims of performing at the optimum level. All subtraction results presented operated in two dimensions, and could likely be improved (Guitton, 2005) by incorporating more dimensions in the process.

We pose the subtraction of the predicted multiples from the data as the following linear inversion problem:

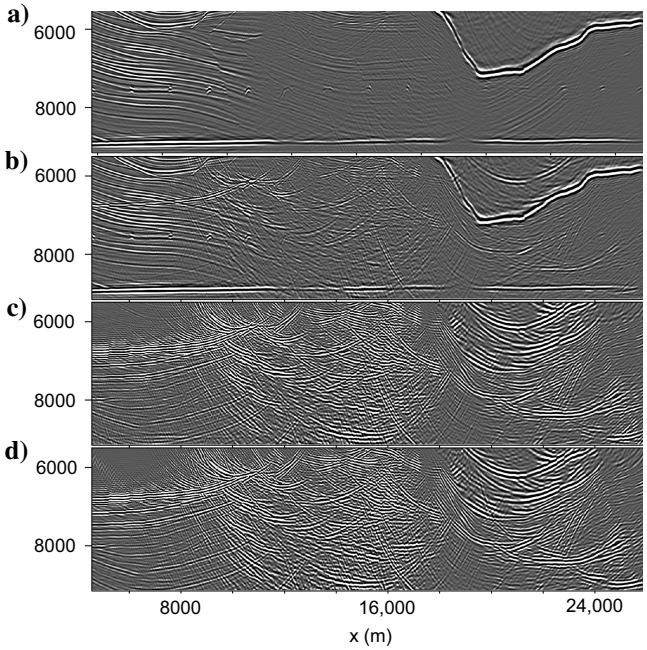

Figure 6. Images of the bottom third of Sigsbee2B modeled data. (a) Migration of primaries only. (b) Migration of multiples and primaries. (c) Migration of multiples only. (d) IS-SRMP image using data containing only primaries.

$$\mathbf{Mf} \approx \mathbf{d} \tag{15}$$

$$\epsilon\mathbf{Af} \approx \mathbf{0} \tag{16}$$

where **M** is the convolutional matrix of the multiples (a matrix whose columns contain shifted versions of a vector of the multiple prediction, **m**), and **f** is a bank of nonstationary filters acting on patches (Claerbout and Fomel, 2002) of the data vector, **d**, which contains primaries and multiples. The matrix **A** is a regularization operator (in this case a Laplacian) and ϵ controls the strength of regularization. The result of this linear inversion is a multiple model, **Mf**, that matches the amplitude and wavelet of the data.

Simple synthetic

Figure 9 details the steps in the subtraction process for an angle-domain common-image gather from the flat-layer synthetic. Figure 9a is the conventional image. Figure 9b panel is the IS-SRMP gather. Figure 9c is the matched version of the IS-SRMP gather. **Mf**, ready to subtract from the image gather. Some energy from the water-bottom primary has leaked into the matched multiple prediction. Where the first multiple crosses the second primary, the filters have difficulty separating the two events. The higher-order multiples at the bottom of the initial prediction have been removed.

Figure 10 contains the final subtraction results. Figure 10a is the subtraction of Figure 9a and c, **d**-**Mf**. This is a reasonable result, but suffers from some artifacts. Figure 10c is the original image gather, **d**. The improved subtraction result in Figure 10b is produced with a second application of the match-filter technique described in equation 15. For this application, the convolutional matrix **M** is made from the subtraction result (Figure 10a), and the data vector **d** is once again the conventional image gather. Therefore, the result shown is the subtraction result matched to the input gather.

Missing data, either source or receiver positions, results in incomplete multiple prediction for SRMP. However, extrapolation spreads

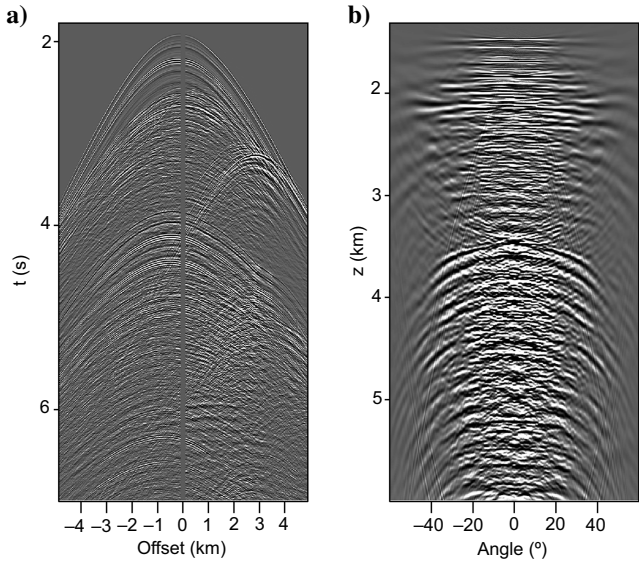

Figure 7. (a) Shot gather from a Gulf of Mexico data set. Near-offset traces are null. Split-spread gathers were created via reciprocity. (b) Subsurface-offset gather from the migrated image at the same location. Subsurface gather contains 1/6 the number of traces in the surface gather.

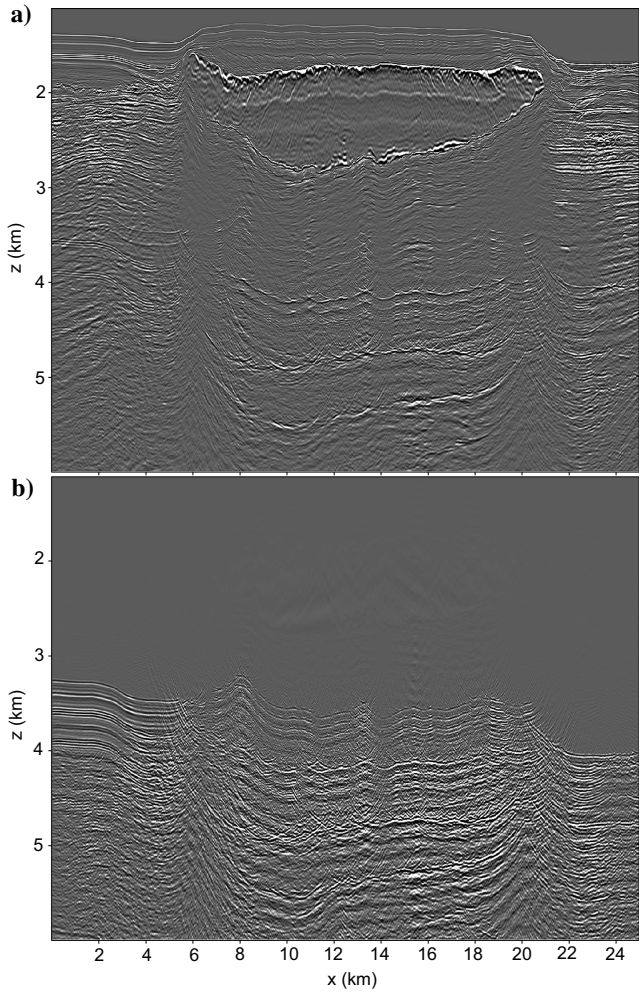

Figure 8. Mississippi Canyon, Gulf of Mexico (a) zero-offset image and (b) the IS-SRMP computed during the course of shot-profile migration of 1096 shots.

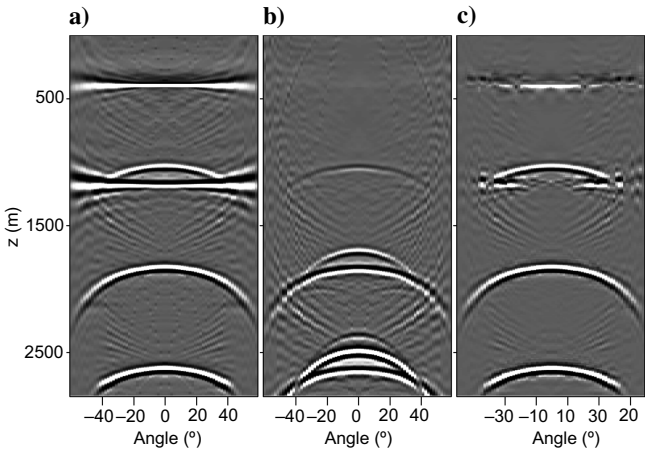

Figure 9. Angle-domain image gathers from a flat-layer model. (a) Conventional image, (b) multiple prediction, and (c) prediction matched to data.

energy across such gaps after a few propagation steps. This is commonly referred to as wavefront healing. Collecting near-offset traces is always difficult in the field. Figures 11 and 12 were produced to test the IS-SRMP algorithm when data does not contain near-offset information. Ten null-traces surrounding the source were substituted in the gather shown in Figure 2, which corresponds to a gap of 200 m. There is some dimming near zero angle in the primary events, and a small deviation in the continuity of the curvature of the predicted multiples.

In the interest of direct comparison, the adaptive subtraction parameters were kept constant for Figures 10 and 12. The faint energy in Figure 12b above the second reflector indicates that the same parameters for the adaptive subtraction are not as appropriate for this image volume. However, the remainder of multiple energy is easily removed from the final result when the subtraction is better tuned.

Sigsbee2B

Figure 13 shows the bottom third of the zero-offset image produced with the Sigsbee2B synthetic data. Figure 13a is the multiple-contaminated image. Figure 13b is the final result produced by adaptive subtraction of the image-space multiple prediction from the image in Figure 13a. For comparison, Figure 13c is the image produced using data with no multiple reflections. The point diffractors masked in the top image are much better realized in the subtraction result. The multiples in the sedimentary section before $x = 10$ km are almost perfectly removed except for some up-right dipping energy at $x = 7$ km emerging from the basement reflector. Several events between $x = 10$–19 km are much more continuous and interpretable.

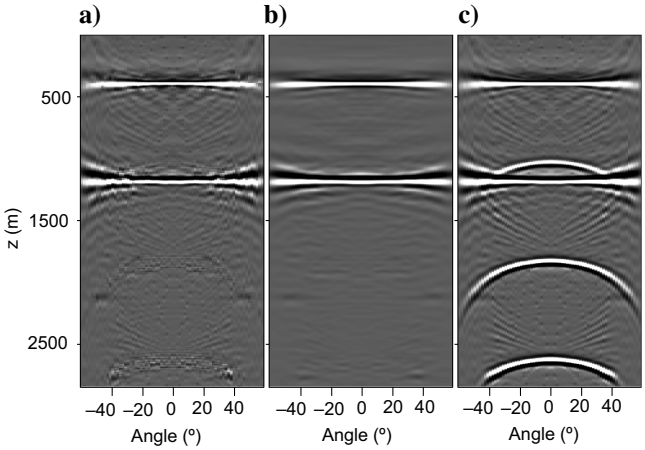

Figure 10. Angle-domain image gathers from a flat-layer model. (a) Subtraction of matched multiple prediction from data, (b) subtraction matched to data, and (c) original data.

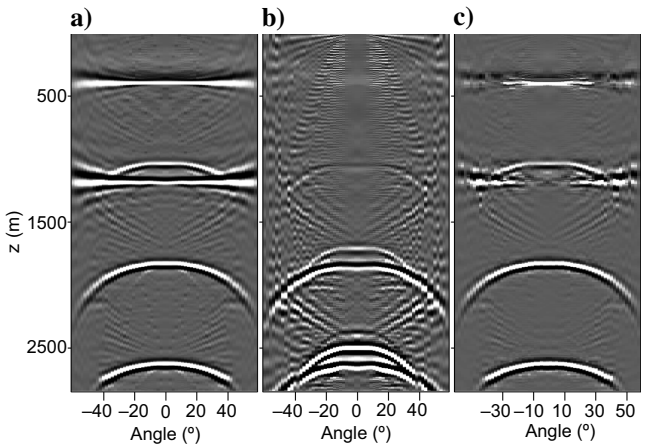

Figure 11. Angle-domain image gathers from a flat-layer model with missing near offsets. (a) Conventional image, (b) multiple prediction, and (c) prediction matched to data.

Gulf of Mexico data

The top panel in Figure 14 shows the bottom half of the multiple contaminated image produced with the Gulf of Mexico data. The center panel is the multiple prediction generated during shot-profile migration. The bottom panel is the subtraction result. The subtraction still contains some residual multiples associated with the salt body. Despite these events being well predicted in the center panel, the residual energy must be due to 3D topography of the top surface of the salt body. It is possible that the result could improve with more diligent adaptive subtraction. Most of the migration diffraction energy associated with the sharp salt edges has been attenuated around $x = 7$ and 20 km. Primaries at $z = 4.5$ km on the left edge of the image have been brought out and may suggest an anticlynal structure.

DISCUSSION

In many geophysical applications, improved results are generated by performing operations in the prestack domain. While more expensive, operating in higher dimensions can often produce better images. Migration performs a sum over frequency, shot position, and (possibly) reflection angle to produce an image volume. We suggest that the amplitude and bandwidth normalization performed in adaptive subtraction can be implemented at the imaging condition using deconvolutional variants (Lee et al., 1991; Guitton et al., 2006). To normalize the frequency content and collapse the wavelet, the imaging condition in equation 3 becomes

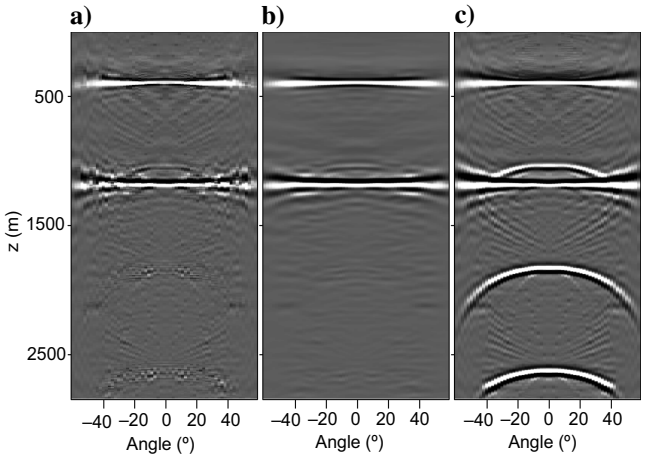

Figure 12. Angle-domain image gathers from a flat-layer model with missing near offsets. (a) Subtraction of matched multiple prediction from data, (b) subtraction matched to data, and (c) original data.

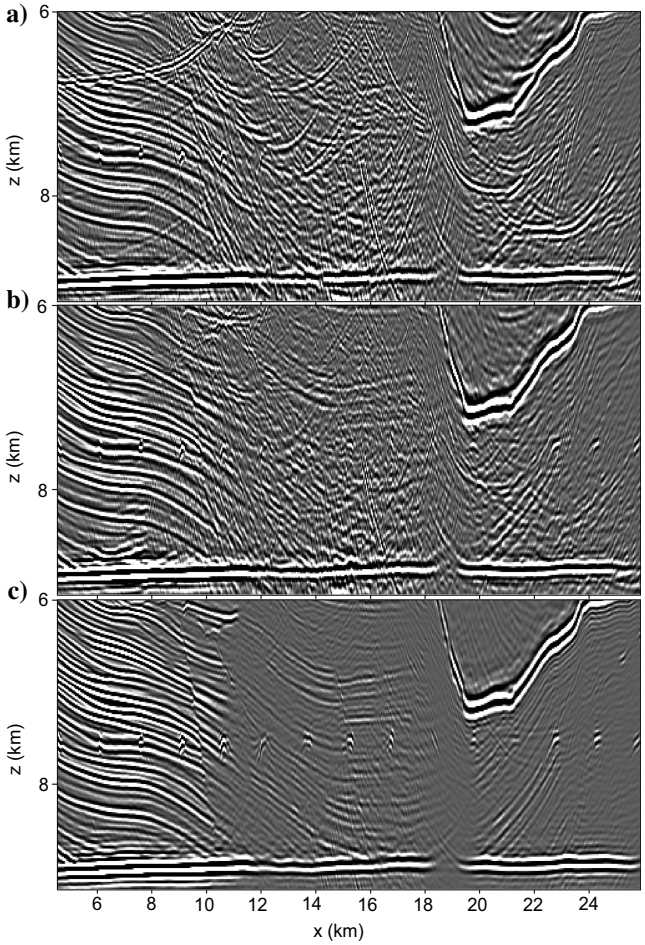

Figure 13. Bottom third of the zero-offset image produced with the Sigsbee2B synthetic data. (a) Image with primaries and multiples, (b) subtraction result, and (c) image produced from data without multiples.

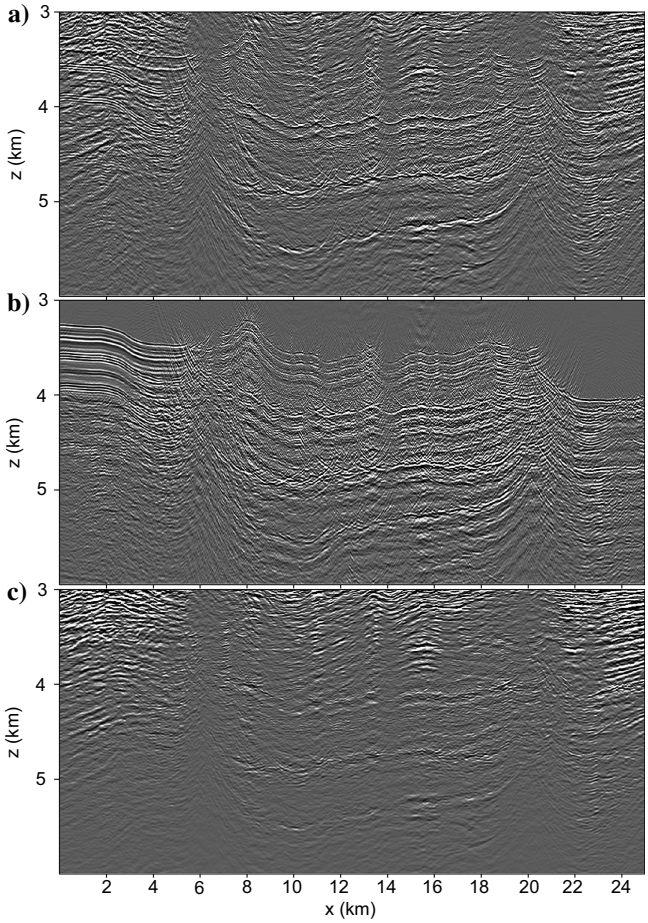

Figure 14. Bottom half of the zero-offset image produced with the Mississippi Canyon, Gulf of Mexico, data provided by Western-Geco. (a) Image with primaries and multiples, (b) image-space multiple prediction, and (c) subtraction result.

$$i_z(\mathbf{x},\mathbf{h}) = \sum_{\mathbf{x}_s}\sum_{\omega} \frac{U_z(\mathbf{x}+\mathbf{h};\mathbf{x}_s,\omega)D_z^*(\mathbf{x}-\mathbf{h};\mathbf{x}_s,\omega)}{\langle\langle D_z(\mathbf{x}-\mathbf{h};\mathbf{x}_s,\omega)D_z^*(\mathbf{x}-\mathbf{h};\mathbf{x}_s,\omega)\rangle\rangle}, \tag{17}$$

where the denominator is smoothed (brackets) across horizontal coordinates for stability. Similarly. the IS-SRMP, equation 9, becomes

$$m_z(\mathbf{x},\mathbf{h}) = \sum_{\mathbf{x}_s}\sum_{\omega} \frac{U_z(\mathbf{x}+\mathbf{h};\mathbf{x}_s,\omega)U_z(\mathbf{x}-\mathbf{h};\mathbf{x}_s,\omega)}{\langle\langle U_z(\mathbf{x}-\mathbf{h};\mathbf{x}_s,\omega)U_z^*(\mathbf{x}-\mathbf{h};\mathbf{x}_s,\omega)\rangle\rangle}. \tag{18}$$

Our experiments to date have not shown this approach particularly effective. There are minor improvements in both zero-offset images, but adaptive subtraction of the multiple prediction is still required. The stability of the multioffset images is very sensitive to the smoothing parameters selected. The deconvolutional variants are substantially more expensive, and have not, so far, proven to be worth the computational burden.

While IS-SRMP, by definition, produces only surface-related multiples, the technique could be manipulated to address strong multiple generators in the subsurface. A layer-stripping type approach derived in parallel to the DSR multiple prediction (Malcolm et al., 2007) could probably be implemented at the cost of extrapolating a third (in addition to the upcoming and down-going) wavefield.

CONCLUSIONS

Image-space SRMP produces a multiple prediction by convolving the data with itself at every subsurface depth level during the course of a shot-profile migration. The result is the same as migrating the conventional data-space multiple prediction (SRMP). This method is most convenient with shot-profile migration strategies since the convolution operation must operate on distinct gathers rather than the combinations thereof produced by resorting to CMP coordinates. The simplicity of this approach can immediately be leveraged to generate the image-space multiple prediction directly from any shot-profile migration program. The method is immediately applicable to 3D, and nonzero subsurface-offset and angle. Any migration algorithm that maintains separate upcoming and down-going wavefields and uses a combinatory imaging condition (e.g., plane-wave and reverse-time migrations) can be easily modified to produce an IS-SRMP volume.

Given a reasonably accurate velocity model for migration, it is only necessary to compute $O(10)$ subsurface offsets. This results in many fewer traces involved in calculating the multiple prediction

than the $O(1000)$ offsets collected at the surface. This savings will be reduced, however, by the need to convolve the traces at every depth level, $O(100)$, of the image space rather than just at the surface. Whatever the balance of floating-point operations for a particular survey, the convenience of being able to generate the multiple prediction during another required processing step can save file manipulation, sorting, and overhead costs. Furthermore, this technique can also be used in a target-oriented fashion simply by not calculating the multiple prediction at shallow depths where it is not required.

Importantly, split-spread gathers must be precomputed via reciprocity for data collected with off-end acquisition geometries. Off-end gathers will not contain (nor therefore predict) emerging rays which pierce the acquisition surface in front of the boat. This may increase the size of the computational domain used for propagating each individual shot-record. The cost increase by performing two imaging conditions is not severe, as the cost of calculating an imaging condition with inline offsets is usually a fraction of the cost of a shot-profile migration. Therefore, whenever a shot-profile migration is being performed, it may be advantageous to generate the IS-SRMP even if a data-space elimination effort has already been performed, especially when the adaptive subtraction leaves some multiple energy in the final result.

The quality of the multiple prediction produced in the image space with this technique is independent of the accuracy of the velocity model used during the migration. The multiple prediction, propagated with the same velocity model, will be kinematically accurate with the location of any multiples in the migrated image. Though both the image and the multiple prediction may be mismigrated, events must correspond when constructed with the same extrapolation operators and velocity model.

Due to the squaring of the wavelet when convolving data, the multiple prediction cannot be directly subtracted from the data or the image. Our adaptive subtraction results show high quality estimations of the primaries for both the Sigsbee2B synthetic and the Gulf of Mexico data examples. Substantial improvement to the estimation of primaries was achieved by reusing the match-filter inversion process to match the subtraction result to the original image. This second iteration mitigates some of the residual energy from the subtraction, restores some of the primary energy inadvertently removed during subtraction, and attenuates some of the artifacts associated with migration and the transform from subsurface offset to angle-domain common-image gathers.

ACKNOWLEDGMENTS

Reviewers C. P. A. Wapenaar, D. J. Verschuur, and Paul Sava all made insightful comments to drafts of this manuscript, that substantially improved its quality.

REFERENCES

Alvarez, G., B. Biondi, and A. Guitton, 2004, Attenuation of diffracted multiples in angle domain common image gathers: 74th Annual International Meeting, SEG, Expanded Abstracts, 1301–1304.

Anstey, N. A., and P. Newman, 1966, The sectional auto-correlogram and the sectional retro-correlogram: Geophysical Prospecting, **14**, no. 4, 389–426.

Baysal, E., D. D. Kosloff, and J. W. C. Sherwood, 1983, Reverse time migration: Geophysics, **48**, 1514–1524.

Berkhout, A. J., and D. J. Verschuur, 1997, Estimation of multiple scattering by iterative inversion, Part I: Theoretical considerations: Geophysics, **62**, 1586–1595.

Biersteker, J., 2001, MAGIC: Shell's surface multiple attenuation technique: 71st Annual International Meeting, SEG, Expanded Abstracts, 1301–1304.

Claerbout, J. F., 1971, Toward a unified theory of reflector mapping: Geophysics, **36**, 467–481.

Claerbout, J., and S. Fomel, 2002, Image estimation by example: Geophysical soundings image construction: Class notes, http://sepwww.stanford.edu/sep/prof/index.html.

Guitton, A., 2005, Multiple attenuation in complex geology with a pattern-based approach: Geophysics, **70**, no. 4, V97–V107.

Guitton, A., A. Valenciano, D. Bevc, and J. Claerbout, 2006, Robust illumination compensation for shot-profile migration: 68th Annual Conference and Exhibition, EAGE, Extended Abstracts, P265.

Hampson, D., 1986, Inverse velocity stacking for multiple elimination: 56th Annual International Meeting, SEG, Expanded Abstracts, 422–424.

Kessinger, W., 1992, Extended split-step Fourier migration: 62nd Annual International Meeting, SEG, 917–920.

Lee, D., I. M. Mason, and G. M. Jackson, 1991, Split-step fourier shot-record migration with deconvolution imaging: Geophysics, **56**, 1786–1793.

Malcolm, A. E., M. V. de Hoop, and H. Calandra, 2007, Identification of image artifacts due to internal multiples: Geophysics, this issue.

Muijs, R., 2005, Wavefield decomposition and imaging of multicomponent seabed seismic data: Ph.D. thesis, Utrecht University.

Rickett, J. E., and P. C. Sava, 2002, Offset and angle-domain common image-point gathers for shot-profile migration: Geophysics, **67**, 883–889.

Sava, P., and A. Guitton, 2003, Multiple attenuation in the image space: 73rd Annual International Meeting, SEG, Expanded Abstracts, 1933–1936.

———, 2005, Multiple attenuation in the image space: Geophysics, **70**, no. 1, V10–V20.

Shan, G., and A. Guitton, 2004, Migration of surface-related multiples: Tests on the Sigsbee2B dataset: 74th Annual International Meeting, SEG, Expanded Abstracts, 1285–1288.

Tsai, C. J., 1985, Use of autoconvolution to suppress first-order long-period multiples: Geophysics, **50**, 1410–1425.

Verschuur, D. J., A. J. Berkhout, and C. P. A. Wapenaar, 1992, Adaptive surface-related multiple elimination: Geophysics, **57**, 1166–1177.

Weglein, A. B., 1999, Multiple attenuation: An overview of recent advances and the road ahead: The Leading Edge, **18**, no. 1, 40–44.